JOM, Vol. 73, No. 2, 2021
https://doi.org/10.1007/s11837-020-04515-8

THERMODYNAMIC OPTIMIZATION OF CRITICAL METALS PROCESSING AND RECOVERY

Investigation of Solid-State Carbothermal Reduction of Fayalite with and Without Added Metallic Iron

HONGYANG WANG,[1,3,4] LEITING SHEN,[2,5] HUANJUN BAO,[1] WENTAO ZHANG,[1] XUAN ZHANG,[1] LIQUN LUO,[1,3] and SHAOXIAN SONG[1,3]

01.—School of Resources and Environmental Engineering, Wuhan University of Technology, Wuhan 430070, China. 02.—School of Metallurgy and Environment, Central South University, Changsha 410083, Hunan, China. 03.—Hubei Key Laboratory of Mineral Resources Processing and Environment, Wuhan University of Technology, Wuhan 430070, Hubei, China. 4.–e-mail: hywang3@whut.edu.cn. 5.–e-mail: shenleiting@csu.edu.cn

Copper slag (CS) with Fe-bearing fayalite and magnetite is the main waste generated during the pyrometallurgical processing of metallic copper. In this paper, the solid-state reduction kinetics of fayalite with and without addition of 10 wt.% metallic iron were studied using the isothermal method. The phase transformation of fayalite was verified by x-ray diffraction, scanning electron microscopy, and energy dispersive spectrometer. Results show that the carbothermal reduction of fayalite is controlled by phase boundary reaction (tridimensional shape), and the activation energy decreases from 165.22 kJ mol^{-1} to 145.74 kJ mol^{-1} after adding 10 wt.% metallic iron. During the carbothermal reduction process, fayalite decomposes into metallic iron and quartz solid solution, followed by the conversion of quartz solid solution into cristobalite solid solution with increasing temperature. The addition of metallic iron creates a nucleating effect and accelerates the decomposition of fayalite. This work contributes to efforts to optimize the carbothermal reduction of CS.

INTRODUCTION

Pyrometallurgy and hydrometallurgy processes are the main methods of extracting copper from copper concentrate, with the pyrometallurgy process accounting for 80% of world extraction.[1] However, 2.0–3.0 tons of copper slag (CS) are generated for every ton of metallic copper produced by the pyrometallurgy process, and the annual generation of CS reaches 40–50 million tons globally.[2,3] Normally, 35–45% Fe and 25–35% SiO_2 are present in CS, whereas the total amount of other ingredients, including Al_2O_3, CaO, MgO, Zn, Pb, and Cu, is less than 10%. Therefore, CS could be used to produce building materials and abrasives,[4,5] but its large-scale treatment is still a problem due to the presence of Zn, Pb, and Cu. At present, iron extraction from the CS is considered to be an efficient method of realizing resource utilization.[6,7]

Fayalite and magnetite are the main Fe-bearing phases in CS, with the mass ratio of fayalite to magnetite in the range of 5–15.[8] Magnetite is a kind of ferromagnetic material that could be recovered by magnetic separation, but the obtained magnetic concentrate is difficult to use as a feedstock for ironmaking due to the presence of Zn and Pb.[9] Given that fayalite is an iron orthosilicate with an olivine crystal structure, separating iron and silicon is difficult. The common methods of decomposing fayalite include acid leaching,[10,11] oxidation roasting,[12,13] and carbothermal reduction.[14–17] During the acid leaching process, the iron and silicon in fayalite enter into the solution and the residue, respectively, but equipment corrosion, wastewater generation and solid–liquid separation are the drawbacks of this method. Fayalite could be converted into hematite and silica by oxidation roast-

(Received July 15, 2020; accepted November 30, 2020; published online January 2, 2021)

ing, then the silica can be removed by alkali leaching.[12] However, the obtained hematite concentrate could not be used as a raw material for iron extraction in the steelmaking industry due to the enrichment of Zn, Pb, and Al in the leaching residue. When fayalite is treated by carbothermal reduction, the decomposition products, ferromagnetic metallic iron and non-magnetic silica, can be easily separated by magnetic separation. Therefore, carbothermal reduction is the most popular method of treating CS, and the Zn and Pb in the CS are enriched in the dust from this process.[14]

According to the Gibbs energies of reactions listed in Eqs. (1) and (2),[18] the reduction of magnetite into metallic iron at a temperature range of 720–1250°C is easier than that of fayalite into metallic iron and silica. Therefore, the metallic iron from magnetite reduction may have an effect on the decomposition of fayalite when treating CS by carbothermal reduction. The kinetics of carbothermal reduction of CS[19–21] and the growth kinetics of iron grains[22] have been systematically studied. However, most of the previous studies only focused on the isothermal kinetics of liquid fayalite at 1250–1450°C[19] or the isothermal kinetics of CS.[20,21] Few studies have reported on the solid-state reduction kinetics of fayalite with and without metallic iron as an additive.

$$Fe_3O_4 + 4C = 3Fe + 4CO,$$
$$\Delta G^\circ = -0.66 * (T/^\circ C) + 475.76\,(\mathrm{kJ\,mol^{-1}}, 0-1400\,^\circ C) \quad (1)$$

$$Fe_2SiO_4 + 2C = 2Fe + SiO_2 + 2CO,$$
$$\Delta G^\circ = -0.32 * (T/^\circ C) + 255.69\,(\mathrm{kJ\,mol^{-1}}, 0-1400\,^\circ C) \quad (2)$$

In this work, the solid-state reduction kinetics of fayalite with and without the addition of 10 wt.% metallic iron were investigated via carbothermal reduction by using coal as a source of carbon. The phase transformation during reduction and the morphology of reduced specimens were analyzed via x-ray diffraction (XRD), scanning electron microscopy (SEM), and energy dispersive spectrometer (EDS). The mechanism of solid-state reduction of fayalite is also discussed. This work contributes to the optimization of CS during carbothermal reduction.

EXPERIMENTAL

Materials

The hematite [$d(0.5)$=2.80 μm], metallic iron [d (0.5)=14.42 μm] and quartz [$d(0.5)$=20.27 μm] powders used in this study were of analytical grade. Fayalite was synthesized under a reducing atmosphere by using hematite, metallic iron, and quartz powders with a stoichiometric ratio in accordance with Eq. (3) at 1250°C for 120 min[23] The obtained fayalite was then ground in a vibrating mill.

$$2Fe_2O_3 + 2Fe + 3SiO_2 = 3Fe_2SiO_4 \quad (3)$$

The coal powder used as reductive reagent was from Wuhan Iron and Steel Company Limited, China. The properties of coal powder, including proximate analysis and the main chemical composition of coal ash, are listed in Table S1 in the supplementary material.

Carbothermal Reduction

Ten grams of fayalite and 2.2 g of coal powder were well mixed in a grinder (XPM–φ120 × 3). The fixed carbon in the coal powder has the main thermodynamic effect on the decomposition of fayalite during carbothermal reduction. Thus, 1.5 times the stoichiometric proportion of coal powder was added to convert fayalite into metallic iron and silica on the basis of the conversion of fixed carbon into carbon monoxide. Considering that the mass ratio of fayalite to magnetite in CS was 5–15, 1 g metallic iron was added into the mixture of fayalite and coal powder to investigate the effect of metallic iron on the carbothermal reduction of fayalite. The mixture of fayalite and coal powder, with and without 10 wt.% metallic iron, was wetted by adding water and pressed into specimens with a size of Φ 15 mm × 5 mm under 20 MPa. Afterwards, the specimens were dried in an oven at 105°C for 5 h.

The carbothermal reduction experiments were undertaken in a thermostatic muffle furnace (SX2-8-16) with a maximum temperature of 1600°C. The specimens of fayalite with and without addition of metallic iron were placed at the bottom of a 100-mL corundum crucible, which was full of coke powder to guarantee a reducing atmosphere during the roasting. When the preset temperature was reached, the corundum crucible was placed into the muffle furnace to realize the carbothermal reduction of fayalite. After a certain period, the corundum crucible was taken out from the furnace and cooled to room temperature. The total iron and metallic iron contents in ground reduced specimens were measured via chemical analysis in accordance with the national standards (GB/T 6730.5-2007 and GB/T 38812.2-2020). The reduction degree of fayalite without adding metallic iron was calculated using Eq. (4). The metallic iron in the mixture of fayalite and coal powder with 10 wt.% metallic iron did not change before and after the carbothermal reduction. Thus, the reduction degree of fayalite with added 10 wt.% metallic iron was calculated in accordance with Eq. (5).

$$RD_1 = \frac{MF_1}{TF_1} \times 100 \quad (4)$$

$$RD_2 = \frac{MF_2 - \frac{7.57 \times m_a}{m_b}}{TF_2 - \frac{7.57 \times m_a}{m_b}} \times 100 \quad (5)$$

where TF_1 and TF_2 are the total iron content in reduced specimens of fayalite (%); MF_1 and MF_2 are the metallic iron content in reduced specimens of fayalite (%); 7.25 is the metallic iron content in the mixture of fayalite and coal powder with 10 wt.% metallic iron (%); and m_a and m_b are the mass of mixture of fayalite and coal powder with 10 wt.% metallic iron and reduced specimens (g).

Analysis Methods

The phase composition of fayalite and the reduced specimens were characterized by a rotation anode powder x-ray diffractometer (MAX-RB, Rigaku Corporation, Japan) using Cu-Kα radiation (λ= 1.5406 Å) with a step size of 0.02°, and the 2 theta (degree) interval was 5°–75°. The microstructure of the specimens were observed on a scanning electronic microscope (JXA-8230, JEOL, Japan) equipped with an INCA X-Act energy dispersive spectrometer. After fixing with epoxy resin and triethanolamine, the specimens were polished and then coated with C to improve the electrical conductivity before SEM–EDS analysis. SEM images were obtained with secondary electrons at 15 kV acceleration voltage and a scan speed of 6. EDS analysis was performed with backscatter electrons at 15 kV acceleration voltage and a working distance of 12 mm. The qualitative chemical composition was measured by EDS X-ray point analysis with an acquisition time of 60 s and analyzed with INCA Energy 350 processing software. The software was calibrated using a Co optimization standard for quantification. Particle size distribution (PSD) was measured using a Mastersizer 2000 (Malvern, UK) particle size analyzer. The size distribution of metallic iron particles was obtained by analyzing the SEM images of reduced specimens with Image-Pro Plus 6.0 software. The chemical compositions were analyzed by an atomic absorption spectrometer (CONTRAA-700, Analytik Jena AG, Germany).

RESULTS AND DISCUSSION

Characteristics of Fayalite

The XRD pattern, PSD and SEM–EDS images of synthesized fayalite are shown in Fig. 1. Figure 1a indicates that the fayalite showed a good crystallization and high purity, with no other detected impurity phase. After grinding, the mean particle size of fayalite was 26.69 μm, and 90% of the particle sizes were less than 71.33 μm, as presented in Fig. 1b. The SEM image and corresponding EDS mapping of element analysis are shown in Fig. 1c and d, respectively. The fayalite demonstrated uniform microstructure, and the element compositions were O, Fe, and Si with an atom ratio of 3.96:2.06:1.00, which was close to the stoichiometric atom ratio of Fe_2SiO_4.

Carbothermal Reduction of Fayalite

The specimens of fayalite with and without addition of metallic iron were reduced in the temperature range of 950–1150°C with an interval of 50°C. The results of the degree of reduction are presented in Fig. 2. The reduction degree of fayalite strongly depended on the roasting temperature and time. In other words, enhancing the temperature and prolonging the heating time could increase the reduction degree. Without addition of metallic iron [Fig. 2a], the reduction degree of fayalite only reached 11.47% at 950°C for 180 min, but remarkably increased with time at 1000°C. When the temperature exceeded 1050°C, the reduction degree of fayalite was already very high by 60 min; then the increase rate slowed down between 60 and 180 min. In accordance with the unreacted shrinking core model, the fayalite particle surface could be quickly reduced into metallic iron and silica due to its close contact with coal powder. By contrast, the reduction of fayalite in the interior of the particle was inhibited by the formed layer of metallic iron and silica.

The reduction degree of fayalite with addition of metallic iron [Fig. 2b] exhibited a similar trend to that seen without addition of metallic iron [Fig. 2a]. The reduction degrees of fayalite in Fig. 2b were slightly higher than those in Fig. 2a. Therefore, metallic iron has a positive influence on the decomposition of fayalite during carbothermal reduction.

Solid-State Reduction Kinetics

In this study, the reduction degree of fayalite was calculated by analyzing the total iron and metallic iron contents in the reduced specimens. This analysis is more accurate than the use of mass loss of the mixture of CS and coal powder measured in some studies.[20,21] In the isothermal reduction process, the kinetics of the solid-state reaction can be expressed as Eq. (6).[24,25]

$$G(\alpha) = \int_0^t A \exp\left(-\frac{E}{RT}\right) dt = kt \quad (6)$$

where $G(\alpha)$ is the integral form of the reaction models, t is the time (min), k is the rate constant, A is the pre-exponential factor (min^{-1}), E is the apparent activation energy ($kJ\ mol^{-1}$), R is the gas constant ($J\ mol^{-1}\ K^{-1}$), and T is the absolute temperature (K).

The generally used solid reaction models listed in Table I were selected to identify the kinetic model, rate controlling steps, and Arrhenius activation energy by linear fitting with the experimental data in Fig. 2. The fitting results showed that the regression coefficient of function $R_3(a)$ was the best among all the models, indicating that the carboth-

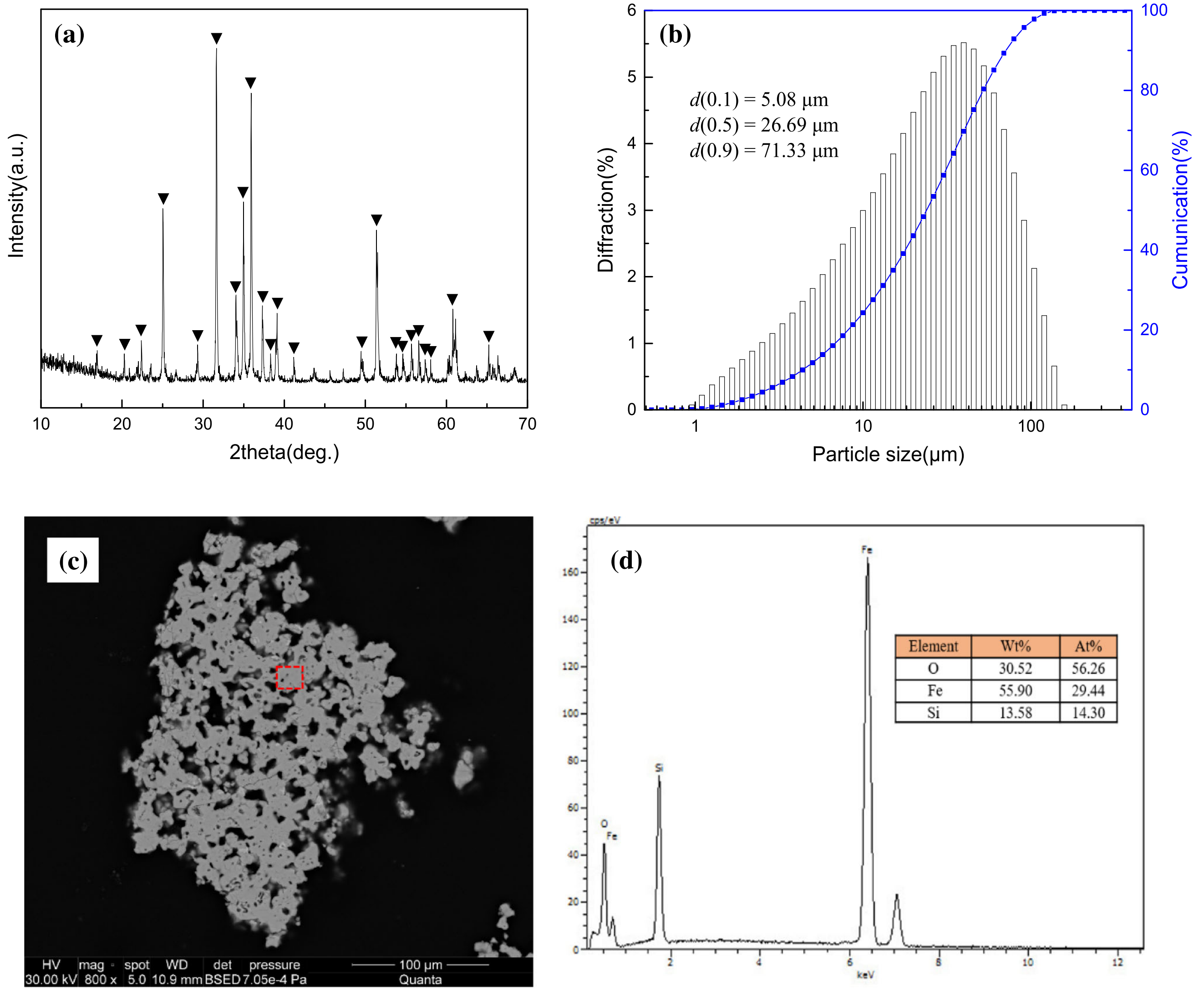

Fig. 1. XRD pattern (a), PSD (b) and SEM–EDS (c, d) of synthesized fayalite. ▼ = Fayalite.

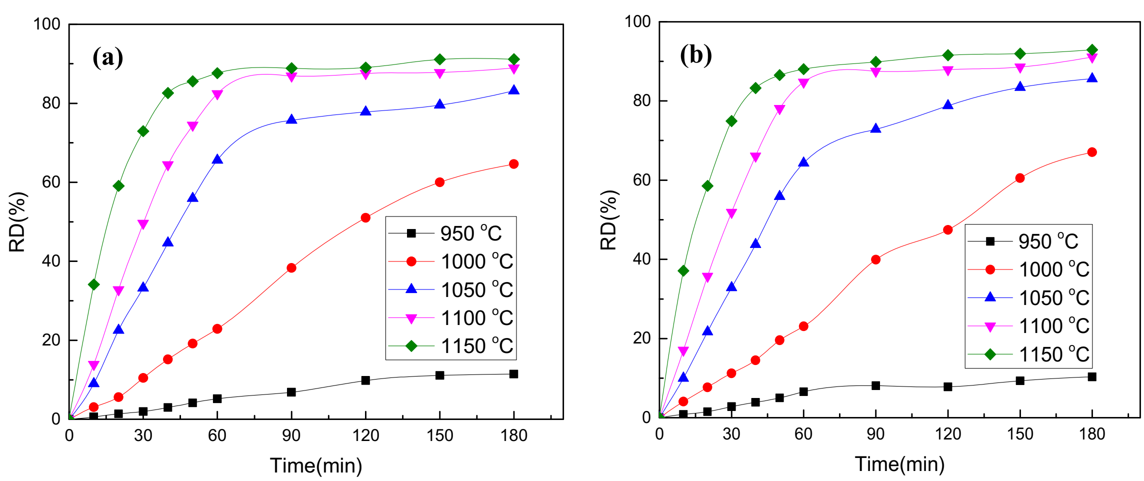

Fig. 2. Reduction degree of fayalite without (a) and with (b) addition of metallic iron at various temperatures and times.

Table I. The general solid reaction models applied[26,27] together with their mean fitting regression coefficient (R^2) calculated in this work

Function	G(a)	Reaction mechanism	Mean fitting regression coefficient (R^2): Adding metallic iron	Mean fitting regression coefficient (R^2): Without adding metallic iron
$A_1(a)$	$-\ln(1-a)$	One-dimensional growth of nuclei (Avrami-Erofeev) n = 1	0.9848	0.9827
$A_2(a)$	$[-\ln(1-a)]^{1/2}$	Two-dimensional growth of nuclei (Avrami-Erofeev) n = 1/2	0.9458	0.9610
$A_3(a)$	$[-\ln(1-a)]^{1/3}$	Three-dimensional growth of nuclei (Avrami-Erofeev) n = 1/3	0.8508	0.8726
$C_1(a)$	$1-(1-a)^{1/4}$	Chemical reaction control n = 1/4	0.9884	0.9875
$C_2(a)$	$1-(1-a)^2$	Chemical reaction control n = 1/2	0.9303	0.9442
$R_2(a)$	$1-(1-a)^{1/2}$	Phase-boundary controlled (contracting cylinder) n = 1/2	0.9869	0.9902
$R_3(a)$	$1-(1-a)^{1/3}$	Phase-boundary controlled (contracting cylinder) n = 1/3	0.9912	0.9927
$D_1(a)$	a^2	One-dimensional diffusion	0.9289	0.9262
$D_2(a)$	$(1-a)\ln(1-a)+a$	Two-dimensional diffusion	0.9159	0.9148
$D_3(a)$	$[1-(1-a)^{1/3}]^2$	Three-dimensional diffusion (Jander equation)	0.8933	0.8901
$D_4(a)$	$1–2/3a-(1-a)^{2/3}$	Three-dimensional diffusion (Ginsteing-Brounshtein equation)	0.9152	0.9075

ermal reduction of fayalite is controlled by phase boundary reaction (tridimensional shape).

In accordance with function $R_3(a)$, the relationship between $1-(1-a)^{1/3}$ and time of the reduced fayalite without and with addition of metallic iron is shown in Fig. 3. The results showed that $1-(1-a)^{1/3}$ had a preferable linear relationship and the reduction degree of fayalite fit well with the theoretical curve of $R_3(a)$ in the first 60 min at 950–1150°C.

The Arrhenius activation energy of the reduced fayalite without and with addition of metallic iron was obtained by calculating the slope of lines in Fig. 3 versus $1/T$, the results of which are shown in Fig. 4. The activation energy of fayalite by carbothermal reduction was 165.22 kJ mol^{-1}, it decreased to 145.74 kJ mol^{-1} after adding 10 wt.% metallic iron. Therefore, the addition of metallic iron could accelerate the decomposition of fayalite during carbothermal reduction by reducing the activation energy of fayalite. In addition, the activation energy of fayalite (165.22 kJ mol^{-1}) was significantly higher than that of CS (118.06 kJ mol^{-1}) as reported in the literature.[20] This finding could be explained by the reduction of magnetite into metallic iron being easier than that of fayalite into metallic iron and silica during the carbothermal reduction of CS.

Phase Transformation During Carbothermal Reduction

The specimens that had been reduced for 90 min in Fig. 2 were analyzed by XRD, and the results are shown in Fig. 5. When the specimens of fayalite with and without addition of metallic iron were roasted at 1000–1050°C for 90 min, the characteristic diffraction peaks of fayalite were observed in all the reduced specimens, and the diffraction peaks of fayalite decreased with the increase in temperature. The characteristic diffraction peaks of fayalite vanished in the XRD patterns of the reduced specimens at ≥1100°C, indicating that efficient decomposition of fayalite was achieved by carbothermal reduction. In the reduced specimens at 1000°C and 1050°C, quartz and cristobalite were also detected, and their diffraction peaks increased as the temperature increased. The enhancement of temperature benefited the conversion of quartz into cristobalite, because the diffraction apexes of cristobalite increased, whereas that of quartz decreased in the XRD patterns of reduced specimens. The quartz and cristobalite detected in the reduced specimens were named quartz solid solution and cristobalite solid solution, respectively, due to their solubility in NaOH solution,[28,29] which can also be verified by the alkali leaching results in Fig. S1 from the supplementary material. The diffraction peaks of metallic iron consistently increased with the enhancement of temperature. Therefore, fayalite first decomposed into metallic iron and quartz solid solution during carbothermal reduction, and then quartz solid solution converted into cristobalite solid solution at increased temperature. The efficient transformation of natural quartz into cristobalite occurred through roasting at 1500°C,[30] while it happened at 1100°C during the carbothermal reduction of fayalite. This result verified that the properties of quartz and cristobalite in reduced specimens differed from the natural quartz and cristobalite.

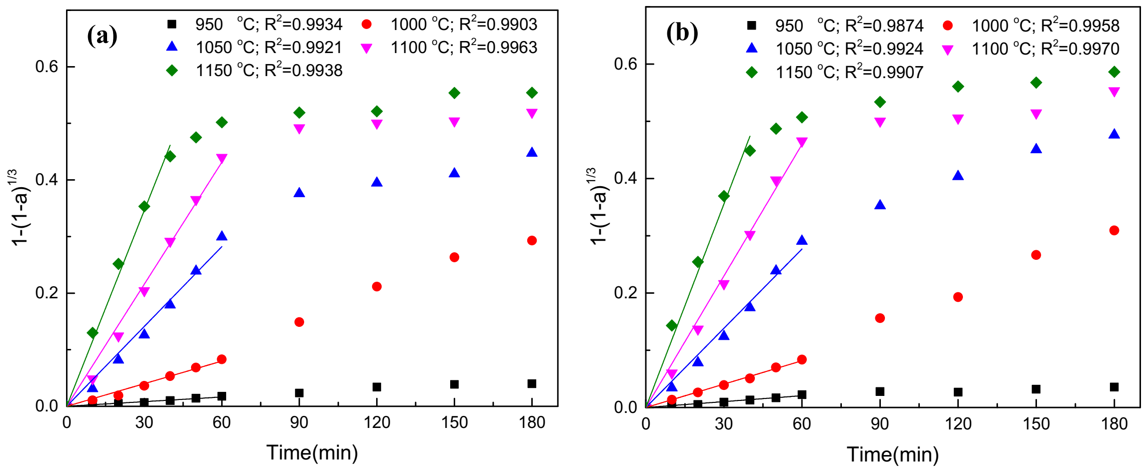

Fig. 3. Relationship between $1-(1-a)^{1/3}$ and time of the reduced fayalite without (a) and with (b) addition of metallic iron.

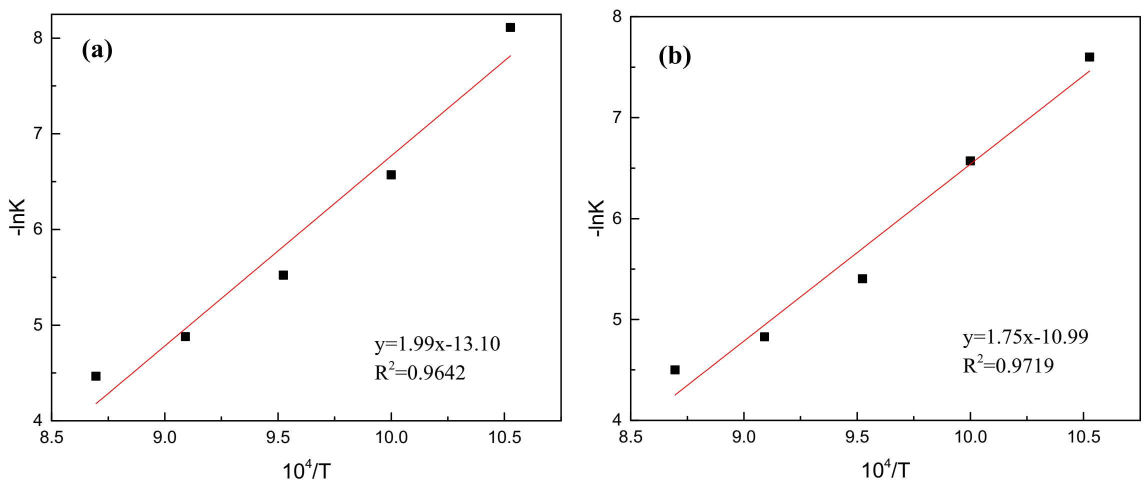

Fig. 4. Arrhenius plots of $-\ln K$ versus $10^4/T$ of R_3(a) kinetic function for the reduced fayalite without (a) and with (b) addition of metallic iron.

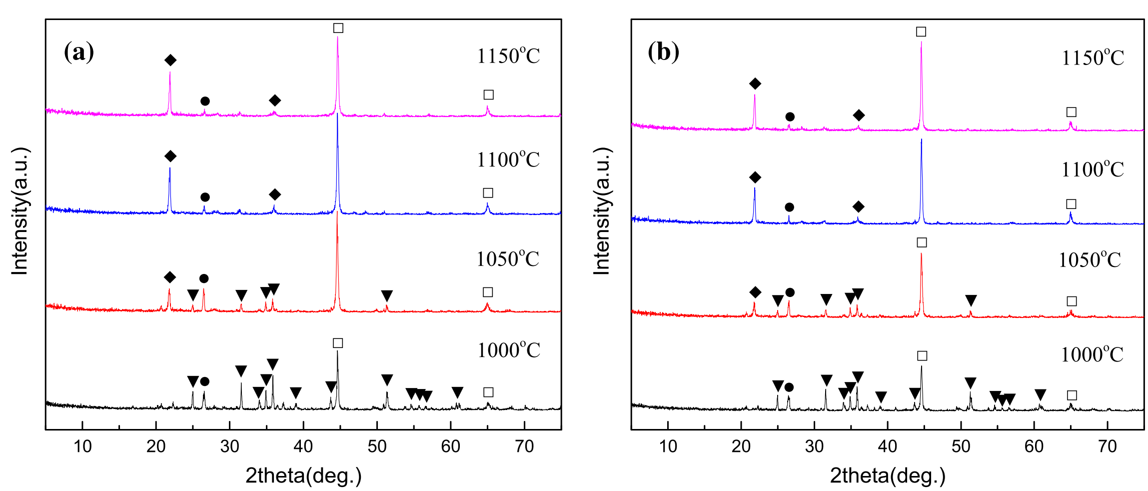

Fig. 5. XRD patterns of reduced specimens without (a) and with (b) addition of metallic iron at various temperatures for 90 min. Symbols: ▼ fayalite, □ cristobalite solid solution, ● quartz solid solution, and □ metallic iron.

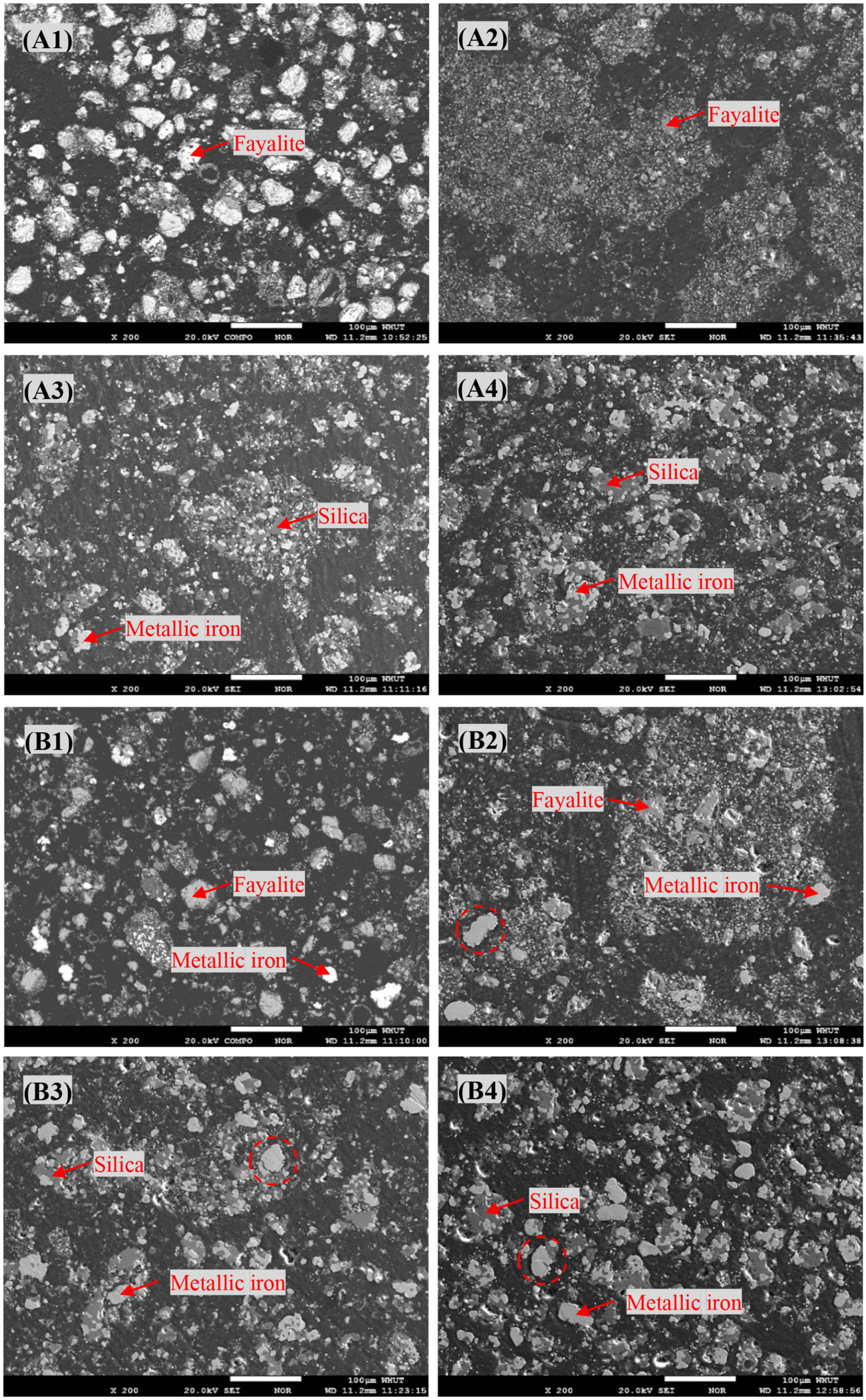

Fig. 6. SEM-EDS of reduced specimens without (a) and with (b) addition of metallic iron at different temperatures for 90 min (*1*, 1000°C; *2*, 1050°C; *3*, 1100°C; *4*,1150°C).

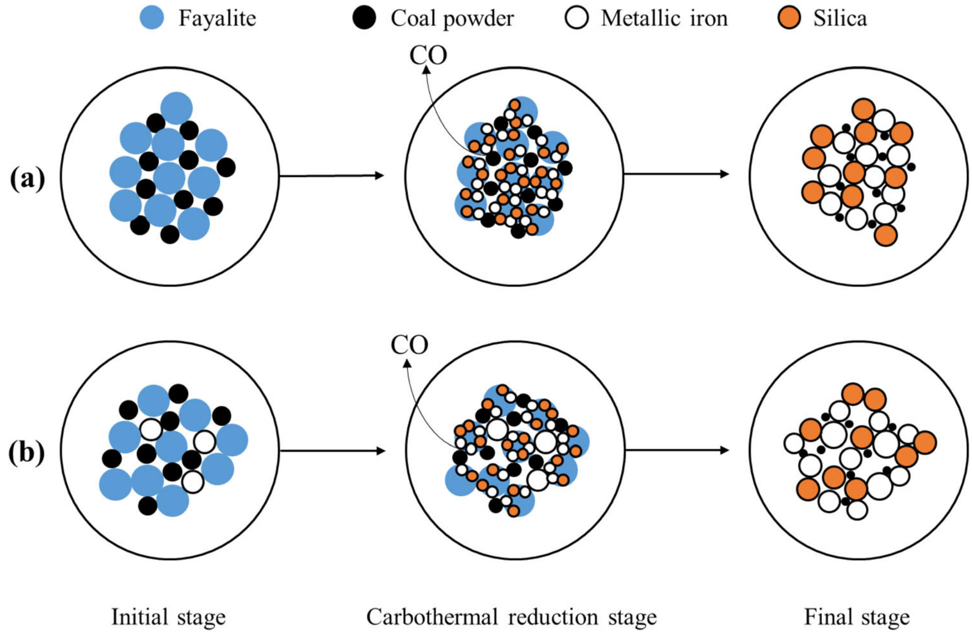

Fig. 7. Schematic illustration of carbothermal reduction of fayalite without (a) and with (b) addition of metallic iron.

Morphology of Reduced Specimens

The morphology of the reduced specimens with and without addition of metallic iron at 1000–1150°C for 90 min was analyzed by SEM–EDS, and the results are shown in Fig. 6. The decomposition of fayalite into metallic iron and silica remarkably enhanced with an increase in roasting temperature from 1000°C to 1050°C [Fig. 6a], as microgranular metallic iron particles were found in the reduced specimens. Independent particles of metallic iron and silica were found in the reduced specimens at 1100°C and 1150°C, with the metallic iron wrapped by silica. Analysis via Image-Pro Plus 6.0 software showed that the average particle sizes of metallic iron were 5.78 μm and 7.09 μm in the reduced specimen at 1100°C and 1100°C, respectively, as shown in Fig. S2 from the supplementary material. Thus, the extraction of metallic iron from the reduced specimens by the traditional grinding-magnetic separation process remained difficult.

Independent particles of metallic iron and unreacted fayalite were found in the reduced specimen at 1000°C, as shown in Fig. 6(B1). When the roasting temperature was increased to 1050°C [Fig. 6 (B2)], the carbothermal reduction of fayalite markedly increased due to the presence of microgranular metallic iron particles in the reduced specimen. In addition, the microgranular metallic iron form the decomposition of fayalite was found on the surface of metallic iron. As shown in Figs. 6(B3) and (B4), independent silica particles around the coarse metallic iron particles were detected, which could be attributed to the added metallic iron presenting a nucleating effect.

Mechanism Analysis

During the carbothermal reduction of fayalite without addition of metallic iron, the fayalite was decomposed into metallic iron and silica by reacting with carbon. An elevated temperature accelerated the heterogeneous nucleation and growth of metallic iron and silica. However, the mean particle size of metallic iron in the reduced specimens was less than 10 m due to the restriction of silica. The added metallic iron presented a nucleating effect in the growth of metallic iron from the decomposition of fayalite, leading to the promotion of fayalite decomposition during carbothermal reduction. A schematic illustration of carbothermal reduction of fayalite with and without addition of metallic iron is shown in Fig. 7.

CONCLUSION

The solid-state reduction kinetics of fayalite with and without addition of 10 wt.% metallic iron were investigated under isothermal conditions, and the reduced specimens were analyzed to disclose the mechanism of adding metallic iron in accelerating the carbothermal reduction of fayalite. The main findings in the work are:

(1) The carbothermal reduction of fayalite was controlled by a phase boundary reaction (tridimensional shape). The addition of metallic iron presented a nucleating effect and accelerated the decomposition of fayalite. The activation energy for carbothermal reduction of fayalite decreased from 165.22 kJ mol^{-1} to 145.74 kJ mol^{-1} with the addition of 10 wt.% metallic iron.

(2) During the carbothermal reduction process, fayalite decomposed into metallic iron and quartz

solid solution, and then the quartz solid solution converted into cristobalite solid solution with increasing temperature. The presence of silica hindered the growth of metallic iron particles.

ACKNOWLEDGEMENTS

This work was financially supported by the China Postdoctoral Science Foundation (2019M662733), National Natural Science Foundation of China (51874219) and National Key Research and Development Program of China (2018YFC1901502).

CONFLICTS OF INTEREST

On behalf of all authors, the corresponding author states that there is no conflict of interest.

REFERENCES

1. M.E. Schlesinger, M.J. King, K.C. Sole, and W.G. Davenport, *Extractive metallurgy of copper* (Elsevier, 2011).
2. Y. Feng, Q.X. Yang, Q.S. Chen, J. Kero, A. Andersson, H. Ahmed, F. Engström, and C. Samuelsson, *J. Cleaner Prod.* 1112 (2019).
3. K. Holland, R.H. Eric, P. Taskinen, and A. Jokilaakso, *Miner. Eng.* 133, 35 (2019).
4. I. Alp, H. Deveci, and H. Sungun, *J. Hazard. Mater.* 159, 390 (2008).
5. B. Gorai, R.K. Jana, and Premchand, *Resour. Conserv. Recycl.* 39, 299 (2003).
6. T.J. Chun, G. Mu, Z. Di, H.M. Long, C. Ning, and D. Li, *Arch. Metall. Mater.* 63, 299 (2018).
7. Z.Q. Guo, D.Q. Zhu, J. Pan, and F. Zhang, *JOM* 68, 2341 (2016).
8. X.S. Lai and H.J. Huang, *Metal Mine* 11, 205 (2017).
9. K.X. Jiao, J.L. Zhang, Z.J. Liu, C.L. Chen, and F.H. Liu, *Ironmaking Steelmaking* 44, 344 (2017).
10. H.S. Altundogan, M. Boyrazli, and F. Tumen, *Miner. Eng.* 17, 465 (2004).
11. A.N. Banza, E. Gock, and K. Kongolo, *Hydrometallurgy* 67, 63 (2002).
12. S. Gyurov, N. Marinkov, Y. Kostova, D. Rabadjieva, D. Kovacheva, C. Tzvetkova, G. Gentscheva, and I. Penkov, *Int. J. Miner. Process.* 158, 1 (2017).
13. I. Gaballah, S. El Raghy, and C. Gleitzer, *J. Mater. Sci.* 13, 1971 (1978).
14. Z.Q. Guo, D.Q. Zhu, J. Pan, W.J. Yao, W.Q. Xu, and J.N. Chen, *JOM* 69, 1688 (2017).
15. J.H. Heo, B.S. Kim, and J.H. Park, *Metall. Mater. Trans. B* 6, 1352 (2013).
16. S.W. Li, J. Pan, D.Q. Zhu, Z.Q. Guo, J.W. Xu, and J.L. Chou, *Powder Technol.* 347, 159 (2019).
17. Z.Q. Guo, J. Pan, D.Q. Zhu, and F. Zhang, *JOM* 70, 150 (2018).
18. I. Barin, *Thermochemical Data of Pure Substances* (Weinheim: VCH Verlagsgesellschaft mbH, 1995).
19. A. Warczok and T.A. Utigard, *Can. Metal. Q.* 37, 27 (1998).
20. H. Zhang, G. Wang, S.H. Zhang, J.S. Wang, and Q.G. Xue, *Nonferrous Metals Sci. Eng.* 10, 28 (2019).
21. L. Zhang, Y. Zhu, W.Z. Yin, B. Guo, F. Rao, and J.G. Ku, *ACS Omega* 5, 8605 (2020).
22. L. Zhang, H.H. Chen, R.D. Deng, W.R. Zuo, B. Guo, and J.G. Ku, *Powder Technol.* 367, 157 (2020).
23. D. Daval, D. Testemale, N. Recham, J.M. Tarascon, J. Siebert, I. Martinez, and F. Guyot, *Chem. Geol.* 275, 161 (2010).
24. A. Khawam and D.R. Flanagan, *J. Phys. Chem. B* 110, 17315 (2006).
25. M.J. Starink, *Thermochim. Acta* 404, 163 (2003).
26. S. Nasr and K.P. Plucknett, *Energy Fuels* 28, 1387 (2014).
27. P.E. Sánchez-Jiménez, A. Perejón, J.M. Criado, M.J. Diánez, and L.A. Pérez-Maqueda, *Polymer* 51, 3998 (2010).
28. X.B. Li, H.Y. Wang, Q.S. Zhou, T.G. G.H. Qi, Liu, Z.H. Peng, and Y.L. Wang, *Trans. Nonferrous Met. Soc. China* 29, 416 (2019).
29. X.B. Li, H.Y. Wang, Q.S. Zhou, T.G. Qi, G.H. Liu, and Z.H. Peng, *Waste Manage.* 87, 798 (2019).
30. A.C.D. Chaklader and A.L. Roberts, *J. Am. Ceram. Soc.* 44, 35 (1961).